

CHEMISTRY

A European Journal

A Journal of



Accepted Article

Title: Halogenated Alkyltetrazoles for Rational Design of Fe(II)-Spin Crossover Materials - Fine-tuning of the Ligands Size

Authors: Danny Müller, Christian Knoll, Marco Seifried, Jan M Welch, Gerald Giester, Michael Reissner, and Peter Weinberger

This manuscript has been accepted after peer review and appears as an Accepted Article online prior to editing, proofing, and formal publication of the final Version of Record (VoR). This work is currently citable by using the Digital Object Identifier (DOI) given below. The VoR will be published online in Early View as soon as possible and may be different to this Accepted Article as a result of editing. Readers should obtain the VoR from the journal website shown below when it is published to ensure accuracy of information. The authors are responsible for the content of this Accepted Article.

To be cited as: *Chem. Eur. J.* 10.1002/chem.201704656

Link to VoR: <http://dx.doi.org/10.1002/chem.201704656>

Supported by
ACES

WILEY-VCH

FULL PAPER

Halogenated Alkyltetrazoles for Rational Design of Fe(II)-Spin Crossover Materials – Fine-tuning of the Ligands Size

Danny Müller,^{*[a]} Christian Knoll,^[a] Marco Seifried,^[a] Jan M. Welch,^[b] Gerald Giester,^[c] Michael Reissner,^[d] Peter Weinberger^[a]

Abstract: 1-(3-halogenpropyl)-1*H*-tetrazoles and their corresponding Fe(II) spin crossover complexes were investigated in a combined experimental and theoretical study. The halogen substitution was found to positively influence the spin transition, shifting the transition temperature about 70 K towards room-temperature. Halogens located in the ω -position were shown to be too far away from the coordinating tetrazole-moiety to have an electronic impact on the spin transition. The subtle variation of ligand steric demand through a highly comparable series was found to have a comparably large impact on the spin transition behaviour, highlighting the sensitivity of the effect to subtle structural changes.

Introduction

Switchable magneto-optical materials are considered promising key-elements in next-generation miniaturized electro-magnetic devices.^[1] In recent years, many innovative concepts for data storage, switching- and sensing devices based on the intrinsic bistability of spin crossover (SCO) materials have been suggested and discussed.^[2] Therefore, currently, major emphasis is placed on the development of novel multifunctional materials,^[3] combining spin crossover behavior with conductivity,^[4] luminescence,^[5] piezoresistance,^[6] paramagnetism,^[7] host-guest chemistry^[8] and many other molecular features, preferably all of which may be correlated to the spin transition. Regardless of these combinatorial approaches, any potential technological application is dominated by the intrinsic boundary conditions of

spin transition temperature and the abruptness of the spin transition behaviour.^[9] Whereas an abrupt change of the spin state above room-temperature, preferably combined with a large hysteresis, is highly desirable for technological application,^[2, 10] most of the currently known spin crossover compounds undergo the high-spin (HS) – low-spin (LS) transition below room-temperature in a rather gradual or even incomplete fashion. Attempts to simplify the design of promising novel materials by establishing a general rule of thumb for the prediction or at least estimation of SCO behavior for new materials have been limited to date. Except for highly isotopic series^[11] the spin transition behavior is affected by too many variables including solvent,^[12] counter ions,^[11a, 12a, 13] H-bonding networks,^[14] packing in the crystal^[15] etc., to allow for a reliable assessment and rational design.

For a systematic investigation of those individual factors contribution to the spin transition, Fe(II) complexes of N1-substituted tetrazoles have proven highly suitable tools:^[16] Accessible by a variety of different, versatile synthetic approaches^[17] terminal or bridging ligands may be obtained, resulting in 0-3- dimensional structures.^[18] The spin state of the SCO material is easily identified by MIR / FIR spectroscopy,^[18b, 19] as the shift of the isolated tetrazolic ν_{CH} -vibration is directly correlated to the Fe-N4 bond-length and thus the irons' actual spin state. Based on these features, variously substituted N1-tetrazoles were subject of choice for several groups, working on a systematic approach for designing SCO materials with a spin transition around room-temperature.

Building on Gütlich's work on $[\text{Fe}(\mathbf{3Tz})_6](\text{BF}_4)_2$ ^[16b, 20] featuring an abrupt, complete spin transition at 130 K with a small hysteresis, a series of terminal and bridging alkyl-tetrazoles with various alkyl-chain lengths were prepared. The longer tails on the tetrazoles resulted in a kind of shock-absorber effect, reducing the internal cooperativity of the system and resulting in only partial spin transitions without any significant increase in $T_{1/2}$. Finally, halogenation of the 1-ethyl-1*H*-tetrazole^[21] was found to be a useful modification of the ligand, raising the spin transition temperature $T_{1/2}$ of its Fe(II)-SCO complex about 70 K as compared to the alkyl-substituted equivalent.^[21b] Based on the infrared spectra and donor number calculations on the halogenated ligands, the impact of the halogen was identified as purely steric, since the halogen-substituent is too far away from the coordinating N4-atom to interfere with its electronics.

To ascertain whether this halogen-substitution of an alkyl-tetrazole could provide a general tool for improving the sterics of the ligand (leading to a positive shift of the spin transition temperature), the 1-propyl-1*H*-tetrazole (**3Tz**) was halogenated in the ω -position, allowing for investigation of the spin crossover

- [a] Dr. Danny Müller, Christian Knoll, Marco Seifried, Priv.Doiz. Dr. Peter Weinberger
Institute of Applied Synthetic Chemistry, TU Wien
Getreidemarkt 9/163-AC, 1060 Vienna, Austria
E-mail: danny.mueller@tuwien.ac.at
- [b] Dr. Jan M. Welch
Atominstut, TU Wien
Stadionallee 2, 1020 Vienna, Austria
- [c] Ao.Univ.Prof. Dr. Gerald Giester
Department of Mineralogy and Crystallography
University of Vienna, Althanstraße 14 (UZA 2), 1090 Vienna, Austria
- [d] Ao.Univ.Prof. Dr. Michael Reissner
Institute of Solid State Physics, TU Wien
Wiedner Hauptstraße 8-10/050, 1040 Vienna, Austria

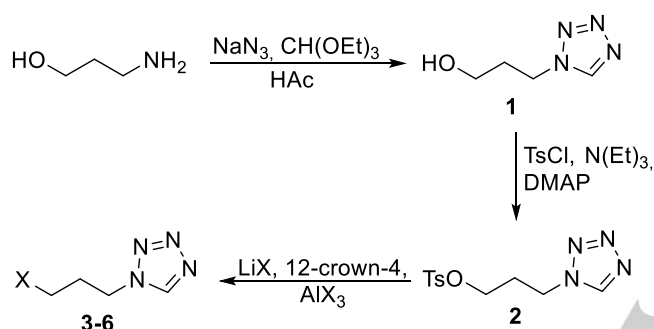
Supporting information for this article is given via a link at the end of the document.

FULL PAPER

properties of $[\text{Fe}(\text{3-X-3Tz})_6](\text{BF}_4)_2$ derivatives of the $[\text{Fe}(\text{3Tz})_6](\text{BF}_4)_2$.

Results and Discussion

To synthesize the ω -halogenated 1-propyl-1*H*-tetrazoles, a divergent synthetic approach based on halogenation of the tosylate **2** was attempted (scheme 1). Although the final halogenation step under microwave conditions was successful, only poor yields around 12 % could be obtained. This was attributed to the presence of the tetrazole - probably due to its Lewis basic properties, - which has previously proven problematic in ligand functionalization.^[22]



X = F (**3**), Cl (**4**), Br (**5**), I (**6**)

Scheme 1. Synthesis of the halogen-substituted 1-propyl-1*H*-tetrazoles

Therefore, an alternative approach based on the Franke-synthesis was selected,^[16] avoiding any further functionalization. For **3-5** the necessary halogenated propylamine is commercially available, whereas for **6** a Finkelstein-reaction of **5** with NaI led to the iodo-derivative (see experimental for further details). On complexation with $\text{Fe}(\text{BF}_4)_2 \cdot 6\text{H}_2\text{O}$ the corresponding Fe(II)-complexes were obtained as colorless solids, all of which change color to bright magenta when cooled in liquid nitrogen.

Magnetic Susceptibility

In figure 1 the temperature dependent magnetic susceptibilities of compounds **7-11** are shown.

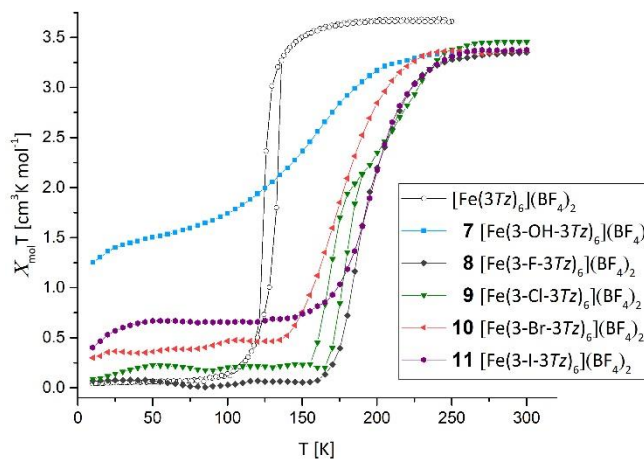


Figure 1. Magnetic susceptibilities of Fe(II)-complexes **7-11**, including the data of $[\text{Fe}(\text{3Tz})_6](\text{BF}_4)_2$ as reference.

Whereas all halogen-containing materials feature a nearly complete spin transition, the hydroxy-substituent in complex **7** causes a very gradual and incomplete transition between 50 and 200 K. Although, the hydroxy-groups in the complex were initially expected to act as hydrogen-bonding partner, thus buffering cooperativity and enhancing the abruptness of the spin transition, its presence was shown to be unfavorable according to the magnetic data. In contrast to the halogenated ethyl-derivatives,^[21b] no correlation between spin transition behavior of complexes **8-11** and the increasing size of its halogen is observed. The high-spin fraction remaining after transition increases inversely with halogen atomic number. The fluorine compound (**8**) shows a completely low-spin state whereas the iodine complex (**11**) shows 21 % residual high-spin configuration. The $T_{1/2}$ values in the series are 175 K (Br, **10**), 212 K / 160 K (Cl, **9**), 194 K (F, **8**) and 200 K (I, **11**). Compared to the parent compound $[\text{Fe}(\text{3Tz})_6](\text{BF}_4)_2$ the spin transition temperature could be shifted about 70 K towards room-temperature. The shape of the magnetization curves for **8**, **10** and **11** indicates the presence of only a single magnetic site in the molecules, as the SCO occurs as single-step transition. In contrast, for the Cl-derivative **9** at 180 K and $2.04 \text{ cm}^3 \text{K mol}^{-1}$ the slope of the magnetization curve suddenly changes, decreasing faster than before. According to the 2:1 HS-LS ratio at 180 K, the presence of three different magnetic iron(II)-sites is deduced for **9**. This could also be confirmed by the structural characterization (see below). In **9**, the spin transition of the first iron site happens between 265 K – 180 K, whereas the two remaining iron sites undergo the spin transition within 25 K, reaching the complete LS-state at 155 K. While determining the magnetic susceptibility in heating mode, the second step of the spin transition was found to show a broad 10 K hysteresis between 165 K and 190 K. Above this temperature the heating and cooling curves are again identical, as observed over the whole temperature regime for compounds **8**, **10** and **11**. The exceptional behavior of the chlorine-substituted derivative **9** within this series was also observed in the case of halogenated 1-ethyl-1*H*-tetrazoles, for which $[\text{Fe}(\text{2-Cl-2Tz})_6](\text{BF}_4)_2$ shows a two-step transition and $[\text{Fe}(\text{2-Cl-}$

FULL PAPER

$2Tz)_6](ClO_4)_2$ a two-step transition with a 17 K broad hysteresis in the second step was reported.^[21a] To investigate the impact of the anion, $[Fe(3-Cl-3Tz)_6](SbF_6)_2$ (**12**) was prepared. The magnetic data revealed, that in this case the use of a larger, octahedral weakly coordinating anion deteriorated the SCO-properties, since at a $T_{1/2}$ of 103 K only about 50 % of the material undergoes the LS-transition (see figure S1).

Mössbauer Spectroscopy

To further characterize the magnetic behavior of **9** temperature-dependent ^{57}Fe -Mössbauer spectra were recorded (see figure 2). Due to the modest statistics at higher temperatures, all spectra were analyzed with only two sub-spectra, one doublet for high spin state and one for low spin state of Fe^{2+} . Up to 120 K 80 % of the spectra correspond to the HS state. Between 120 K and 220 K a transition mainly to the LS doublet is observed, ending with approximately 63% LS and 37% HS at room temperature (see figure 3). The transition observed in the Mössbauer spectra is in good agreement with the magnetic susceptibility measurements of **9**. The two-step transition observed in the susceptibility measurements is not visible in the Mössbauer results, as therefore a notably higher measurement density would be necessary. Nevertheless, a strong jump in quadrupole splitting of the HS component $QS = eQV_{zz}/4$ between 120 and 180 K indicates a drastic change in the local surrounding of the Fe-atoms. This observation fits very well with the data obtained from the molecular structure, showing notable changes in the lattice parameters for the same temperature range (see Figure 5). No such change is found for the half width (inset figure 3). To further evaluate the Mössbauer data regarding the three different Fe sites, a detailed analysis with 6 sub-spectra (3 for the LS and 3 for the HS) would be necessary. Based on the insufficient statistics of the measured spectra such detailed evaluation would be afflicted with a high uncertainty, and was therefore avoided.

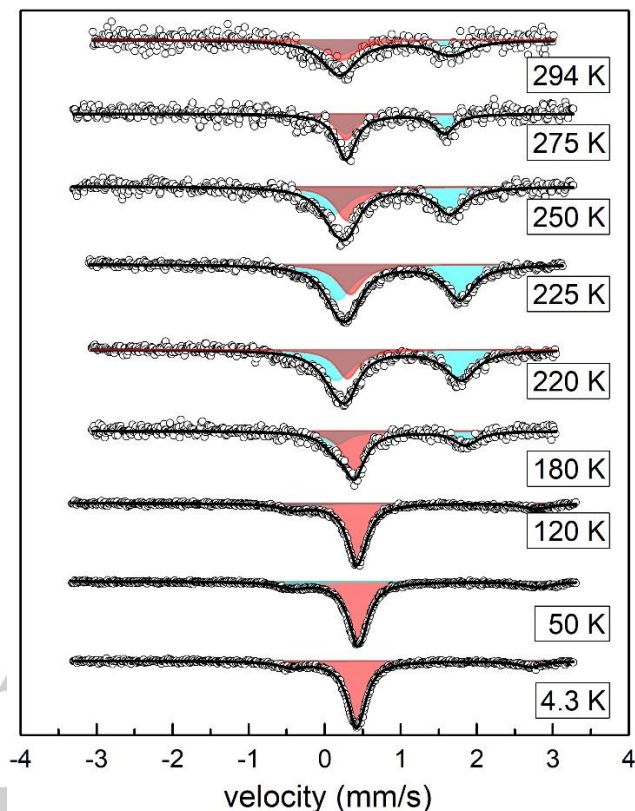


Figure 2. ^{57}Fe -Mössbauer spectra recorded for **9** at different temperatures.

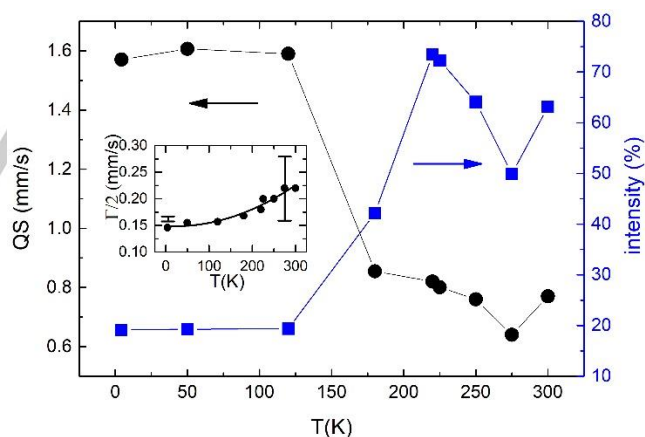


Figure 3. Temperature dependence of the intensity (left) and quadrupole splitting QS (right) for the LS component in the Mössbauer spectra. Inset: temperature dependence of the half width of LS component.

Structural Characterization

For 3-(1*H*-tetrazol-1-yl)propan-1-ol (**1**), the only solid ligand in this study, single crystals were grown by slow evaporation of a CH_2Cl_2 -solution. **1** crystallizes in the triclinic space group $P\bar{1}$ ($N^{\circ} 2$) as crystallographically unique molecule on a general position and two formula units per cell (see figure 4).

FULL PAPER

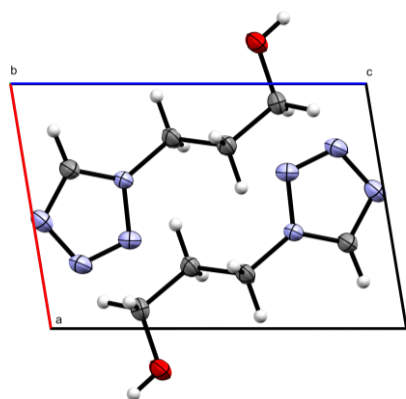


Figure 4. Molecular structure of 3-(1*H*-tetrazol-1-yl)propan-1-ol (**1**), view along the crystallographic *b*-axis at 200 K. Details on the structure determination are found in table S1.

Many attempts and various techniques were used to grow single crystals suitable for structural characterization of compounds **8-12**. Finally, only for $[\text{Fe}(\text{3-Cl-3Tz})_6](\text{BF}_4)_2$ very small, hexagonal platelets could be obtained by diffusion of Et_2O into a MeCN solution, combined with slow evaporation of the solvents. The structure was determined at three different temperatures, covering the most interesting temperatures of the magnetic measurement. The reason for the two-step spin-transition was found in a splitting of the iron positions, corresponding to a crystallographic phase-transition, resulting in expansion of the unit cell. In figure 5 the temperature dependent variation of cell parameters and angles are compared with the magnetic susceptibility of **9**. Accompanying the onset of the spin transition, a structural transformation and symmetry loss occurs, transforming the structure from the former trigonal space group $R\bar{3}$ ($N^\circ 148$) of the high-spin state to the triclinic space group $P\bar{1}$ ($N^\circ 2$) for the mixed HS-LS state. Upon reaching the complete low-spin state, lower symmetry is retained, concomitant with a further distortion of the unit cell. In table S1 and S2-S4 the corresponding crystallographic data, as well as representative angles and bond-lengths are listed.

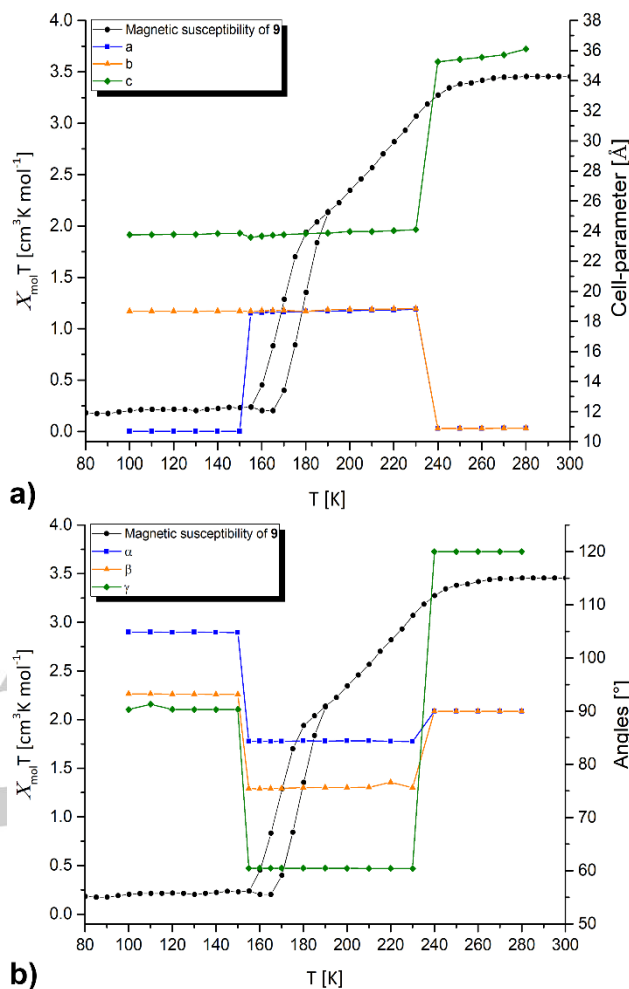


Figure 5. Magnetic susceptibility of **9** correlated to a) temperature dependent variation of the cell-parameters b) temperature dependent variation of the angles

At room-temperature the structure of **9** possesses a magnetically unique iron position with the iron atom coordinated by 6 1-(3-chloropropyl)-1*H*-tetrazoles with a Fe-N4 distance of 2.194 Å characteristic for an Fe(II) HS-state. The large thermal ellipsoids for the ω -carbon of the propyl-chain (C4) and the Cl-atom seen in figure 6 are caused by a free thermal motion in the solid/ local disorder of the 3-chloropropyl chains. In the unit cell three different iron locations on the Wyckoff position 3b, having the site symmetry group $\bar{3}$ are found. The BF_4^- anions are disordered, relating two different orientations of the tetrahedron by a pseudo mirror-symmetry with the mirror-plane parallel to (001). The anions establish a network of $\text{H}\cdots\text{F}$ bonds between the anions and the H-atom of the tetrazole rings, which is observed for all three measured structures.

FULL PAPER

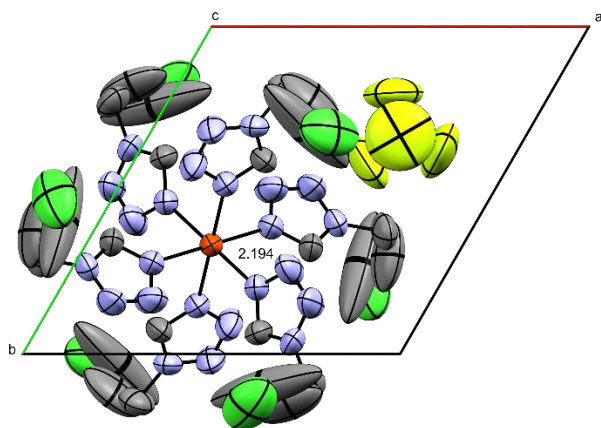


Figure 6. Coordination environment around the Fe-center of **9** in the HS-state at 300 K, view along the crystallographic *c*-axis. For a list of bond-lengths and bond-angles see table S2.

Cooling to 235 K a crystallographic phase transition is observed, splitting the former unique iron position to one position for the LS-state and two positions for the remaining HS-state, both on the Wyckoff position 18f with symmetry 1. Accompanying the change to the triclinic system, the *c*-axis is shortened from 36.116 Å to 23.929 Å, whereas the *a*- and *b*-axis are elongated from 10.900 Å to 18.787 Å. The Fe-N4 distance for the LS-iron is approximately 2.020 Å at 200 K (figure 7), which agrees well with literature known bond-lengths for Fe(II) in the LS-state. Due to the thermal contraction the Fe-N4 bond-length for the HS-state is shortened to around 2.170 Å. Unlike the structure at 300 K, the six Fe-N4 distances and N-Fe-N angles are no longer equal and the bond-lengths mentioned here are representative examples. For a list of bond-lengths and bond-angles see table S3. Nonetheless, for both the ω -carbon of the propyl-chain (C4) and the Cl-atom large thermal ellipsoids are observed.

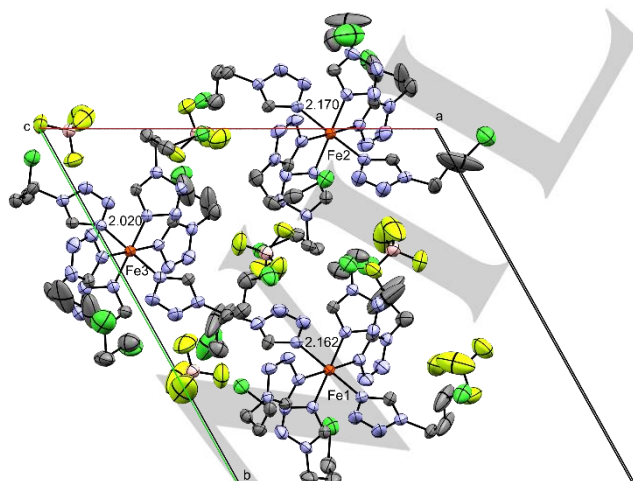


Figure 7. Asymmetric unit of **9** at 200 K, including three different Fe(II)-sites. Fe1 and Fe2 are in the HS-state, Fe3 transformed to the LS-state in the first

step (see figure 1). View along the crystallographic *c*-axis. For a list of bond-lengths and bond-angles see table S3

At 150 K a further structural transformation occurs involving only the *a*-axis (shortened to 10.698 Å) and the unit cell angles. The former three magnetically different Fe(II)-positions are now reduced to two distinguishable positions, having Fe-N4 distances of 1.993 Å (Fe1) and 1.991 Å (Fe2), as shown in figure 8. As for the 200 K structure, the bond-lengths and angles around the iron atoms vary slightly. Both iron positions are still located on the Wyckoff position 18f with symmetry 1. The disorder of the chloropropyl-chains is now limited to one ligand coordinated to the Fe2, which could be refined with a split-position ω -carbon of the propyl-chain (C4) and the Cl-atom, both with a weighting scheme of 0.5

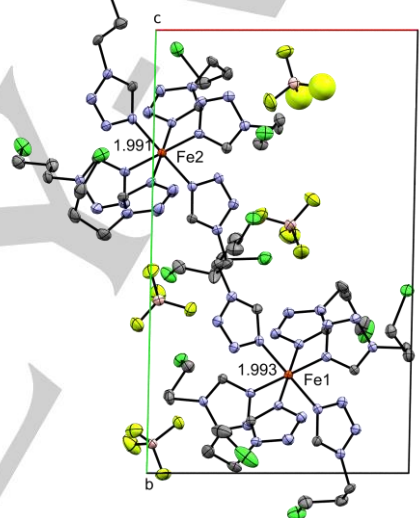


Figure 8. Asymmetric unit of **9** at 120 K, both iron sites in the LS-state, view along the crystallographic *c*-axis. For a list of bond-lengths and bond-angles see table S4.

Infrared Spectroscopy

The characteristic vibrations of the tetrazole-ring are found in the mid infrared around 3130 cm^{-1} (the stretching vibration of the tetrazolic C-H) and 1480-1495 cm^{-1} (the $\nu_{\text{N2=N3}}$ stretching vibration) and are listed for the ligands **1** and **3-6** in table 1. As the energies of the bands in the MIR are very sensitive to the electronic environment, the lack of a systematic shift for the various halogen-substituents confirms their purely steric impact, leaving the electronics of the coordinating tetrazole ring unaffected.

FULL PAPER

Table 1. Comparison of characteristic tetrazolic bands of the ligands

	OH (1) [cm ⁻¹]	F (3) [cm ⁻¹]	Cl (4) [cm ⁻¹]	Br (5) [cm ⁻¹]	I (6) [cm ⁻¹]
ν_{CH}	3130	3136	3135	3134	3131
$\nu_{\text{N=N}}$	1495	1486	1485	1485	1484

Upon coordination the tetrazolic vibrations are affected due to formation of the Fe-N4 bond, resulting in an increase in energy of about 11 – 17 cm⁻¹ in complexes **7-11** (see table 2).

Table 2. Comparison of characteristic tetrazolic bands for the complexes **7-11** in the HS and LS state

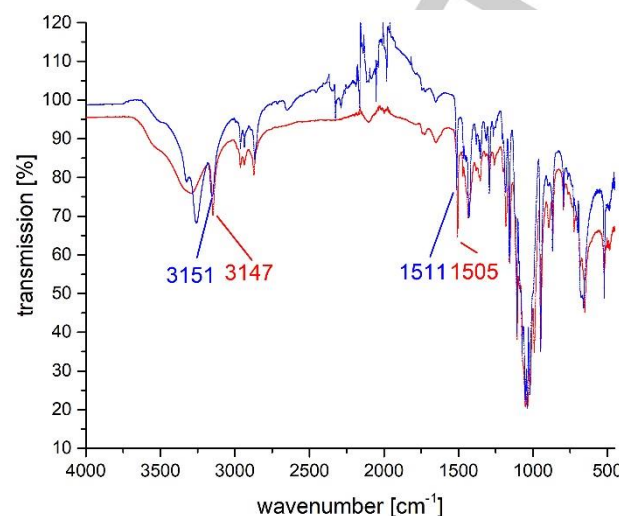
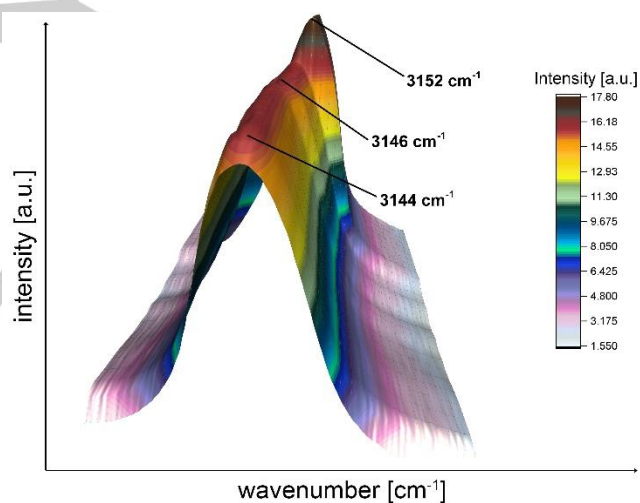
	OH (7) [cm ⁻¹]	F (8) [cm ⁻¹]	Cl (9) [cm ⁻¹]	Br (10) [cm ⁻¹]	I (11) [cm ⁻¹]
ν_{CH} (HS)	3147	3147	3145	3145	3139
ν_{CH} (LS)	3151	3147	3151	3149	3148
$\nu_{\text{N=N}}$ (HS)	1505	1506	1506	1505	1505
$\nu_{\text{N=N}}$ (LS)	1511	1512	1513	1511	1510

Temperature dependent MIR / FIR spectroscopy was used for complementary characterization of the spin-states in complexes **7-12**, as on the HS-LS transition, the bond-strength of the Fe-N4 bond is drastically changed. This results in a shift of the neighboring ν_{CH} and $\nu_{\text{N=N}}$ to higher wavenumbers in the LS-state. Again, as seen by comparison of the vibrational energies in table 2 the shifts and positions are relatively constant over the whole series, excluding any electronic impact of the terminal halogen on the spin transition. In figure 9 representative MIR spectra for [Fe(3-OH-3Tz)₆](BF₄)₂ are compared for the HS and LS state, for **8-12** the spectra are found in figure S3-S7.

In the case of the two-step spin transition observed for [Fe(3-Cl-3Tz)₆](BF₄)₂ the mixed HS-LS state concomitant with the crystallographic phase transition can be monitored in the MIR. Starting at 3144 cm⁻¹ at 298 K in the high-spin state, a shoulder appears for the ν_{CH} -vibration on cooling and splitting to one LS and two HS iron positions. This occurs accompanied by a slight shift to 3146 cm⁻¹. Upon further cooling a more pronounced shift at 155 K to 3152 cm⁻¹ indicates the complete transformation to the LS state. A three-dimensional representation of these effects is given in figure 10. Characteristically for complexes with the BF₄⁻ anion are broad, intense B-F stretching vibrations with a maximum at 1030 cm⁻¹. In the case of **12** a comparable vibration, attributed to the SbF₆⁻ anion is found at 660 cm⁻¹.

Another prominent feature of hexacoordinated Fe(II)-tetrazole complexes is the spin-state dependent vibration of the Fe atom in the N₆-coordination octahedron in the N-N-N planes.^[18b] This more or less decoupled vibrational mode yields either an absorption band around 220 cm⁻¹ for an Fe(II) in high-spin state

and or around 420 cm⁻¹ for the corresponding LS-state. The temperature-dependent FIR spectra for the series are shown in figure S8-S13.

**Figure 9.** Variable temperature MIR spectra of **7** at 298 K (red) and 100 K (blue) with labelled characteristic tetrazolic bands shifted due to the spin transition.**Figure 10.** Stepwise shift of the tetrazolic ν_{CH} during the two-step spin transition of **9**. For a better visibility the spectra are represented in absorption.**UV-VIS / NIR Spectroscopy**

The different spin states of an Fe(II)-complex correlate to a change in the associated electronic transitions. Solid state UV-VIS / NIR spectroscopy in diffuse reflection was used to obtain the ligand-field spectra of the Fe(II)-complexes **7-12** in both spin-states (see figure S13-S18). For Fe(II)-complexes octahedrally coordinated by tetrazoles, in the HS-state at room-temperature the characteristic ⁵T₂ → ⁵E transition occurs around 850 cm⁻¹ in the near infrared, thus invisible for the human eye. In contrast, the

FULL PAPER

${}^1A_1 \rightarrow {}^1T_1$ transition, as well as the ${}^1A_1 \rightarrow {}^1T_2$ transition are both observed in the visible region of the electromagnetic spectrum around 550 cm^{-1} and 380 cm^{-1} and are responsible for the bright magenta color of the LS-state. From the absorption maxima observed in the HS- and LS-spectra the octahedral ligand field strength $10Dq$ of the different compounds may be estimated, as for octahedral complexes with neutral ligands the ligand field correlates with the dipole-moment of the ligand μ and the distance from metal to ligand r (Eq. 1).^[23]

$$10Dq \approx \mu/r^6 \quad (1)$$

This leads to Eq. 2

$$\frac{10Dq^{LS}}{10Dq^{HS}} = \left(\frac{r_{LS}}{r_{HS}}\right)^6 \quad (2)$$

Whereas $10Dq^{HS}$ is directly obtained from the ligand field spectrum in form of the ${}^5T_2 \rightarrow {}^5E$ transition, $10Dq^{LS}$ may be approximated according to Eq. 3.

$$10Dq^{LS} = E({}^1T_1) - E({}^1A_1) + \left(\frac{E({}^1T_2) - E({}^1T_1)}{4}\right) \quad (3)$$

The values for the ligand field strengths of compounds **8-11** listed in table 3. **7** and **12** were omitted, as the spin transitions of both complexes are incomplete.

Table 3. Ligand field strengths of complexes **8-11**

	${}^1A_1 \rightarrow {}^1T_1$ (cm^{-1}) ^[a]	${}^1A_1 \rightarrow {}^1T_2$ (cm^{-1}) ^[b]	$10Dq^{HS}$ (cm^{-1})	$10Dq^{LS}$ (cm^{-1})	$10Dq^{LS} / 10Dq^{HS}$
8	27027	18450	11416	20594	1.80
9	27027	18349	11834	20519	1.73
10	27027	18281	11442	20468	1.79
11	27027	18215	12255	20418	1.67

^[a] $E({}^1T_2)$

^[b] $E({}^1T_1)$

To compare the spectroscopically obtained values for the ligand field strength with the ones obtained from structural parameters, the experimental Fe-N4 distances of **9** in the HS- and LS state were used. According to Eq.1 this results in a value of 1.78 for $10Dq$, which is in reasonable agreement with the values calculated in table 3. Interestingly, for **9** and for **11** a literature value for the ligand field strength of 1.72, obtained from averaged Fe-N4 distances is in better accordance than the current experimental one.

Quantum Chemical Calculations

Quantum chemical calculations were used to theoretically model the impact of the halogens on ligand electronics. In figure 11 the calculated total electron density and the electro static potential for the halogenated propyl-1*H*-tetrazoles **3-6** and the unsubstituted 1-propyl-1*H*-tetrazole (**3Tz**) as reference are shown.

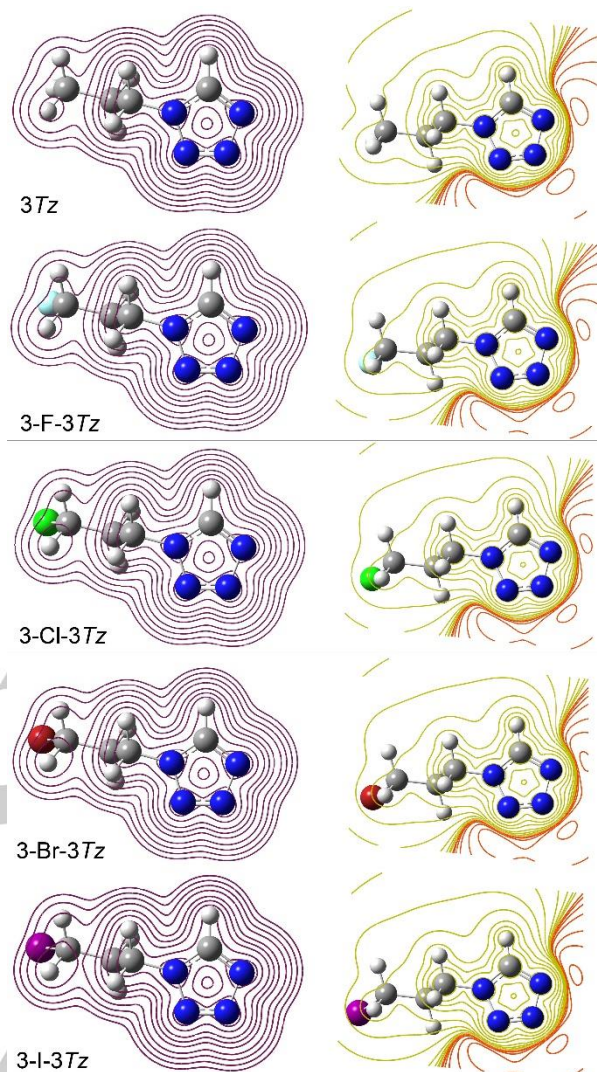


Figure 11. Calculated total electron density (left) and electro static potential (right) for the unsubstituted 1-propyl-1*H*-tetrazole and the halogenated derivatives **3-6**, virtual plane through the tetrazole ring.

Comparing these representations, the only significant difference in the electronics of the various ligands is in the electron density around the halogen. At the tetrazole, and especially the coordinating N4, no significant impact of halogen substitution on the charge distribution is observed. Although, figure 11 represents the potential in a virtual plane parallel to the tetrazole, a similar picture is obtained when a virtual plane parallel to the halogen is used (see figure S19). From the theoretically calculated characteristic vibrations of the halogenated ligands (table S5) and the calculated Mulliken charges of the compounds (table S6), again, no significant differences throughout the series are observed. These theoretical results serve to confirm the experimentally observed behavior of the series thus substantiating the conclusion that the impact of the halogen is purely steric. This small impact on the molecular alignment and

FULL PAPER

packing in the crystal is sufficient to cause the observed variation in the spin transition behavior.

Calculated structures and spectra of the complexes **8-11** as Fe²⁺-cations were used to support the interpretation of the spectra. The calculated structure parameters are in good agreement with experimental findings. In table S7 and S8 the Mulliken charges of selected atoms are compared in both spin-states, again comparable within the series.

Conclusions

In the current study a series of ω -halogenated 1-propyl-1*H*-tetrazoles and their Fe(II) spin crossover complexes were investigated. Compared to an earlier study on halogenated 1-ethyl-1*H*-tetrazole, the sharp and complete spin transition of [Fe(3Tz)₆](BF₄)₂ was used as initial point to verify the hypothesis, halogenation of an alkyl-tetrazole ligand could be used as versatile synthetic tool for in an increase of the spin transition temperature.

For the complete series of OH (**7**), F (**8**), Cl (**9**), Br(**10**), I(**11**) substituted 1-propyl-1*H*-tetrazoles spin crossover active Fe(II)-complexes were obtained, featuring a higher spin transition temperature than the parent compound with a maximal T_{1/2} of 200 K for the iodo-complex **11**. All materials except the Cl-derivative led to a single-step transition. Similarly to the 1-(2-chloroethyl)-1*H*-tetrazole from literature, the 1-(3-chloropropyl)-1*H*-tetrazole also yields a material showing a two-step spin transition, for which the second step shows a 10 K hysteresis. The magnetic transition is concomitant with a crystallographic phase transition at 235 K, for which the structure with a single iron position is transformed from the trigonal system to triclinic with three distinguishable iron positions (2 HS, 1 LS). This process was monitored by temperature dependent crystallography, as well as infrared spectroscopy, both clearly resolving the different spin-states on the iron centers.

In contrast to the literature-known halogenated ethyl-tetrazoles for the propyl-series no clear correlation between increasing spin transition temperature and halogen size / atomic number was found. By a combined experimental and quantum chemical approach it was confirmed, that the halogen substitution has only an impact on the steric demand of the ligand, but does not affect the electronics of the coordinating tetrazole. The approach of a fine-tuning of the spin transition temperature by modification of (N1-substituted alkyltetrazole)-ligands was found successful, demonstrating, how sensitive SCO-systems are to subtle modifications.

Experimental Section

Methodology

If not otherwise stated, all operations involving iron(II) were carried out under inert gas atmosphere (argon 5.0). The glassware used were oven dried at 120 °C before use for at least 2 hours. All solvents for the complexation reactions were dried before use and stored over molecular sieve 3 Å under argon.^[24] Unless otherwise stated, all starting materials

were commercially obtained and used without further purification. All NMR spectra were recorded in dry, deuterated solvents as indicated on a Bruker Avance UltraShield 400 MHz. Chemical shifts are reported in ppm; ¹H and ¹³C shifts are referenced against the residual solvent resonance. The magnetic moment of the Fe(II)-complexes was measured using a Physical Property Measurement System (PPMS[®]) by Quantum Design. The experimental setup consisted of a vibrating sample magnetometer attachment (VSM), bearing a brass-sample holder with a quartz-glass powder container. The moment was determined in an external field of 1 T in the range of 10 K to 300 K. ⁵⁷Fe-Mössbauer measurements were performed with a standard constant acceleration spectrometer in transmission geometry. The ⁵⁷CoRh source was mounted on the driving system and kept at room temperature. Calibration of velocity scale was carried out with α -Fe foil. For temperature variation between 4.2 K and room temperature a continuous flow cryostat was used in which the sample is kept in He exchange gas. Temperature stability was ± 0.5 K at temperatures above 77 K and ± 0.2 K below. The spectra were analysed by solving the full Hamiltonian with both magnetic and electrostatic interaction. Variable temperature solid state UV-Vis-NIR spectra were recorded on a Perkin-Elmer Lambda 900 spectrophotometer between 320 and 1400 nm in diffuse reflectance against BaSO₄ as background. A Harrick coolable/heatable powder sample holder in "Praying Mantis" configuration was used. Variable temperature mid-range (4000 - 450 cm⁻¹) and far-range (700-130 cm⁻¹) infrared spectra were recorded in ATR technique with a Perkin-Elmer Spectrum 400, fitted with a coolable/heatable PIKE Gladi ATR-Unit.^[25] Single crystals were attached to a glass fiber by using perfluorinated oil and were mounted on a Bruker KAPPA APEX II diffractometer equipped with a CCD detector with Mo K α radiation (Incoatec Microfocus Source μ S: 30 W, multilayer mirror, $\lambda=0.71073$ Å). Data of **9** were collected in a dry stream of nitrogen (Cryostream 800, Oxford Cryosystems) at 300 K, for **1** 200 K were used. Redundant data sets up to $2\theta = 55^\circ$ were collected. For the measurements of **9** at 200 K and 120 K a Nonius KappaCCD diffractometer (graphite monochromatized Mo K α -radiation, $\lambda = 0.71073$ Å) equipped with a 0.3 mm monocapillary optics collimator was used. For all measurements data were reduced to intensity values by using SAINT-Plus^[26], and an absorption correction was applied by using the multi-scan method implemented by SADABS.^[26] For the iron(II) complexes, protons were placed at calculated positions and refined as riding on the parent C atoms. All non-H atoms were refined with anisotropic displacement parameters. For thermogravimetric analyses / decomposition of the Fe(II)-complexes a Netzsch Jupiter STA-system with a heating rate of 10 K/min under N₂ atmosphere was used between 25 °C and 450 °C. The powder X ray diffraction measurements were carried out on a PANalytical X'Pert diffractometer in Bragg Brentano geometry using Cu K $\alpha_{1,2}$ radiation, an X'Celerator linear detector with a Ni filter, sample spinning with zero background sample holders and $2\theta = 4-70^\circ$, T = 298 K. A background correction and a K α_2 strip were performed using the PANalytical program suite HighScorePlus v3.0d. The computational results presented were achieved using Gaussian 09 Rev.D01^[27] and visualized using GaussView 5.0.8. The structures of the ligands were drawn using GaussView followed by a molecular mechanics structure optimization implemented in the software package. For the complexes, the molecular structures were imported from the single crystal X-ray analysis to GaussView. The calculations were run using density functional theory with the hybrid functional B3LYP^[28] for structure optimization to a ground state and vibrational modes to prove the discovery of a local minimum. Ligands were optimized with the 6-311++g(d,p) valence triple zeta basis set^[29] with polarization and diffuse functions on all atoms for all elements except halogen atoms where the LanL2DZ^[30] basis set was used for refining the structure. Complexes were optimized using the CEP-121G^[31] basis set as cations, high spin and low spin states were calculated applying the according spin multiplicity.

Synthesis

Tetrazoles and their derivatives are potentially shock sensitive or explosive compounds and should therefore be handled with great care and under appropriate safety precautions!

3-(1*H*-tetrazol-1-yl)propan-1-ol (1): 3-Aminopropan-1-ol (25 g, 0.33 mol, 1 eq.) was suspended together with NaN₃ (32.5 g, 0.5 mol, 1.5 eq.) in a mixture of triethylorthoformate (86 ml, 0.52 mol, 1.55 eq.) and 100 ml

FULL PAPER

acetic acid for 18 h at 95 °C. After cooling, the precipitated salts were separated by filtration and the solvents were removed by evaporation. The residual yellow oil was refluxed for 5 h in 50 ml concentrated hydrochloric acid to decompose the formed 3-(1*H*-tetrazol-1-yl)propyl acetate. On completion, the hydrochloric acid was evaporated and the resulting oil purified by column chromatography on silica gel (MeCN : CH₂Cl₂ = 3:2), to give **1** (15.9 g, 37.4 %) as colourless oil, which crystallized on standing. Mp: 60.8 °C; $\nu_{\text{CH(Tz)}}$ cm⁻¹: 3130; ¹H NMR (400 MHz, CDCl₃, δ): 1.96 – 2.49 (m, 2H), 2.50 (s, 1H), 3.66 (t, J = 5.7 Hz, 2H), 4.63 (t, J = 6.7 Hz, 2H), 8.72 (s, 1H) ppm; ¹³C{¹H} NMR (101 MHz, CDCl₃, δ): 31.92, 45.21, 58.34, 143.23 ppm; EA Calc. for C₄H₈N₄O: C 37.49, H 6.29, N 43.73, O 12.49; found: C 37.43, H 6.44, N 43.83, O 13.41.

3-(1*H*-tetrazol-1-yl)propyl 4-methylbenzenesulfonate (2): **1** (5 g, 39.0 mmol, 1 eq.) was dissolved with 4-toluenesulfonyl chloride (8.1 g, 39.4 mmol, 1 eq.) in 100 ml dry CH₂Cl₂. Then a tiny amount of DMAP was added and the reaction mixture cooled to 0 °C. Triethylamine (10.9 ml, 78.0 mmol, 2 eq.) was added slowly and on complete addition, the mixture was refluxed for 18 h. After removal of all volatiles, the sticky residue was redissolved in CH₂Cl₂ and extracted four times with 100 ml H₂O. After drying over MgSO₄, the solvent was removed and the beige solid recrystallized from CHCl₃ / CCl₄, to give **2** (8.6 g, 78.2 %) as fluffy white needles.

Mp: 76.3 °C; $\nu_{\text{CH(Tz)}}$ cm⁻¹: 3137; ¹H NMR (400 MHz, CDCl₃, δ): 2.21 – 2.35 (m, 2H), 2.39 (s, 3H), 3.68 – 4.08 (m, 2H), 4.49 (t, J = 6.7 Hz, 2H), 7.49 (dd, J = 156.9, 8.0 Hz, 4H), 8.57 (s, 1H) ppm; ¹³C{¹H} NMR (101 MHz, CDCl₃, δ): 21.69, 29.07, 44.27, 65.94, 127.88, 130.13, 132.21, 143.09, 145.54 ppm; EA Calc. for C₁₁H₁₄N₄O₃S: C 46.80, H 5.00, N 19.85, O 17.00, S 11.36; found: C 45.78, H 5.10, N 17.84, O 18.12, S 11.23.

1-(3-fluoropropyl)-1*H*-tetrazole (3): Same procedure as for **1**, 3-Fluoropropylamine hydrochloride (1 g, 8.8 mmol) was used as starting material. Purification of the crude material by column chromatography on silica gel (MeCN : CH₂Cl₂ = 3:2) resulted **3** (160 mg, 14 %) as colourless oil. $\nu_{\text{CH(Tz)}}$ cm⁻¹: 3136; ¹H NMR (400 MHz, CDCl₃, δ): 2.37 (dt, J = 26.4, 6.8, 5.4 Hz, 2H), 4.48 (dt, J = 46.9, 5.5 Hz, 2H), 4.62 (t, J = 6.8 Hz, 2H), 8.64 (s, 1H) ppm; ¹³C{¹H} NMR (101 MHz, CDCl₃, δ): 30.52 (d, J = 20.0 Hz), 44.57 (d, J = 4.7 Hz), 79.98 (d, J = 166.9 Hz), 143.01 ppm; EA Calc. for C₄H₇N₄F: C 36.92, H 5.42, N 43.06, F 14.6; found: C 36.54, H 5.39, N 40.93.

1-(3-chloropropyl)-1*H*-tetrazole (4): Same procedure as for **1**, 3-Chloropropylamine hydrochloride (25 g, 170.6 mmol) was used as starting material. Purification of the crude material by column chromatography on silica gel (MeCN : CH₂Cl₂ = 3:2) resulted **4** (13.2 g, 46.7 %) as colourless oil. $\nu_{\text{CH(Tz)}}$ cm⁻¹: 3135; ¹H NMR (400 MHz, CDCl₃, δ): 2.31-2.38 (m, J = 6.4 Hz, 2H), 3.47 (t, J = 6.1 Hz, 2H), 4.60 (t, J = 6.8 Hz, 2H), 8.82 (s, 1H) ppm; ¹³C{¹H} NMR (101 MHz, CDCl₃, δ): 31.77, 40.83, 45.20, 143.24 ppm; EA Calc. for C₄H₇N₄Cl: C 32.78, H 4.81, N 38.22, Cl 24.19; found: C 33.42, H 5.24, N 32.15.

1-(3-bromopropyl)-1*H*-tetrazole (5): Same procedure as for **1**, 3-Bromopropylamine hydrobromide (25 g, 114.2 mmol) was used as starting material. Purification of the crude material by column chromatography on silica gel (MeCN : CH₂Cl₂ = 3:2) resulted **5** (9.2 g, 42.1 %) as colourless oil. $\nu_{\text{CH(Tz)}}$ cm⁻¹: 3134; ¹H NMR (400 MHz, CDCl₃, δ): 2.37 – 2.64 (m, 2H), 3.34 (t, J = 6.1 Hz, 2H), 4.63 (t, J = 6.7 Hz, 2H), 8.75 (s, 1H) ppm; ¹³C{¹H} NMR (101 MHz, CDCl₃, δ): 31.85, 46.30, 60.65, 143.17 ppm; EA Calc. for C₄H₇N₄Br: C 25.15, H 3.69, N 29.33, Br 41.83; found: C 25.23, H 3.53, N 31.82.

1-(3-iodopropyl)-1*H*-tetrazole (6): **5** (1.5 g, 7.9 mmol, 1 eq.) was dissolved in 50 ml dry acetone. After addition of NaI (1.77 g, 11.8 mmol, 1.5 eq.) the yellow suspension was refluxed for 18 h. All volatiles were removed and the yellow residue extracted with CH₂Cl₂. The crude product was purified by column chromatography on silica gel (MeCN : CH₂Cl₂ = 3:2) resulting **6** (1.2 g, 64.2 %) as slightly yellow oil.

$\nu_{\text{CH(Tz)}}$ cm⁻¹: 3131; ¹H NMR (400 MHz, CDCl₃, δ): 2.39-2.46 (m, J = 6.6 Hz, 2H), 3.10 (t, J = 6.4 Hz, 2H), 4.58 (t, J = 6.7 Hz, 2H), 8.73 (s, 1H) ppm; ¹³C{¹H} NMR (101 MHz, CDCl₃, δ): 32.44, 48.47, 60.67, 143.11 ppm; EA Calc. for C₄H₇N₄I: C 20.18, H 2.96, N 23.54, I 53.31; found: C 20.86, H 3.39, N 24.36.

[Fe(3-OH-3Tz)₆](BF₄)₂ (7): Fe(BF₄)₂·6H₂O (216.4 mg, 0.6 mmol, 1 eq.) and **1** (500 mg, 3.91 mmol, 6.1 eq.) were dissolved in 10 ml MeCN and stirred at 50 °C for 18 h. After evaporation of the solvent the residual oil was triturated in 10 ml CH₂Cl₂ for 1 h to remove the excess of ligand. The CH₂Cl₂-phase was removed and the oily residue dissolved in 5 ml MeCN. By slow addition of Et₂O until the solution became opaque and subsequent cooling at – 30 °C for 12 h **7** was obtained as white solid (214 mg, 33.4 %). $\nu_{\text{CH(Tz)}}$ cm⁻¹: 3147; EA Calc. for C₂₄H₄₈B₂F₈FeN₂₄O₆: C 28.88, H 4.85, B 2.17, F 15.23, Fe 5.59, N 33.68, O 9.62; found: C 27.57, H 4.94, N 32.04. Decomposition: see Figure S20; P-XRD: see Figure S26

[Fe(3-F-3Tz)₆](BF₄)₂ (8): Fe(BF₄)₂·6H₂O (20.5 mg, 61 μ mol, 1 eq.) and **3** (48 mg, 0.37 mmol, 6.1 eq.) were dissolved in 2 ml MeCN and stirred at 50 °C for 18 h. After evaporation of the solvent the residual solid was triturated in 2 ml CH₂Cl₂, resulting **8** as white solid (17.4 mg, 28.0 %). $\nu_{\text{CH(Tz)}}$ cm⁻¹: 3147; EA Calc. for C₂₄H₄₂B₂F₁₄FeN₂₄: C 28.54, H 4.19, B 2.14, F 26.33, Fe 5.53, N 33.28; found: C 28.41, H 3.96, N 31.53. Decomposition: see Figure S21; P-XRD: see Figure S27

[Fe(3-Cl-3Tz)₆](BF₄)₂ (9): Fe(BF₄)₂·6H₂O (188.7 mg, 0.56 mmol, 1 eq.) and **4** (500 mg, 3.4 mmol, 6.1 eq.) were dissolved in 10 ml MeCN and stirred at 50 °C for 18 h. After evaporation of the solvent the residual solid was triturated in 10 ml CH₂Cl₂, resulting **9** as white solid (214 mg, 34.5 %). $\nu_{\text{CH(Tz)}}$ cm⁻¹: 3145; EA Calc. for C₂₄H₄₂B₂Cl₆F₈FeN₂₄: C 26.00, H 3.82, B 1.95, Cl 19.18, F 13.71, Fe 5.04, N 30.31; found: C 25.91, H 3.78, N 29.93. Decomposition: see Figure S22; P-XRD: see Figure S28

[Fe(3-Br-3Tz)₆](BF₄)₂ (10): Fe(BF₄)₂·6H₂O (145.1 mg, 0.43 mmol, 1 eq.) and **5** (501 mg, 2.6 mmol, 6.1 eq.) were dissolved in 10 ml MeCN and stirred at 50 °C for 18 h. After evaporation of the solvent the residual solid was triturated in 10 ml CH₂Cl₂, resulting **10** as white solid (185 mg, 31.3 %). Decomposition: see Figure S22
 $\nu_{\text{CH(Tz)}}$ cm⁻¹: 3145; EA Calc. for C₂₄H₄₂B₂Br₆F₈FeN₂₄: C 20.95, H 3.08, B 1.57, Br 34.85, F 11.05, Fe 4.06, N 24.44; found: C 20.33, H 3.07, N 21.76. Decomposition: see Figure S23; P-XRD: see Figure S29

[Fe(3-I-3Tz)₆](BF₄)₂ (11): Fe(BF₄)₂·6H₂O (64.6 mg, 0.19 mmol, 1 eq.) and **6** (278 mg, 1.2 mmol, 6.1 eq.) were dissolved in 10 ml MeCN and stirred at 50 °C for 18 h. After evaporation of the solvent the residual solid was triturated in 10 ml CH₂Cl₂, resulting **11** as white solid (135 mg, 42.5 %). $\nu_{\text{CH(Tz)}}$ cm⁻¹: 3139; EA Calc. for C₂₄H₄₂B₂I₆F₈FeN₂₄: C 17.39, H 2.55, B 1.30, F 9.17, Fe 3.37, I 45.93, N 20.28; found: C 18.85, H 2.78, N 20.98. Decomposition: see Figure S24; P-XRD: see Figure S30

[Fe(3-Cl-3Tz)₆](SbF₆)₂ (12): FeCl₂·4H₂O (113 mg, 0.57 mmol, 1 eq.) and AgSbF₆ (390.7 mg, 1.14 mmol, 2 eq.) were stirred in 2 ml MeCN for 1 h. The precipitated AgCl was separated and the clear solution added to **4** (500 mg, 3.4 mmol, 6.1 eq.), dissolved in 10 ml MeCN. After stirring at 50 °C for 18 h the solvent was evaporated and the residue triturated in 10 ml CH₂Cl₂, resulting **12** as white solid (384 mg, 48.0 %).

FULL PAPER

$\nu_{\text{CH(Tz)}}$ cm^{-1} : 3160; EA Calc. for $\text{C}_{24}\text{H}_{42}\text{Cl}_6\text{F}_{12}\text{FeN}_{24}\text{Sb}_2$: C 20.49, H 3.01, Cl 15.12, F 16.21, Fe 3.97, N 23.90, Sb 17.31; found: C 19.18, H 2.66, N 21.11. Decomposition: see Figure S25; P-XRD: see Figure S31

Acknowledgements

We acknowledge financial support of the Austrian Science Fund (FWF Der Wissenschaftsfond) project P24955-N28. The computational results presented have been achieved using the Vienna Scientific Cluster, elemental analysis was performed at the Microanalytical Laboratory, Vienna University. Special thanks are to the X-ray center of TU Wien and Dr. Klaudia Hradil. This work was performed in the framework of the Corporation in Science and Technology (COST) action CM1305 "Explicit Control Over Spin-states in Technology and Biochemistry (ECOSTBio).

Keywords: Spin Crossover • Iron • N-ligands • Tetrazoles • Rational Design

- [1] a) A. Bousseksou, G. Molnar, L. Salmon and W. Nicolazzi, *Chemical Society Reviews* **2011**, *40*, 3313-3335; b) C. Lefter, V. Davesne, L. Salmon, G. Molnár, P. Demont, A. Rotaru and A. Bousseksou, *Magnetochemistry* **2016**, *2*, 18; c) C. Lefter, R. Tan, S. Tricard, J. Dugay, G. Molnár, L. Salmon, J. Carrey, A. Rotaru and A. Bousseksou, *Polyhedron* **2015**, *102*, 434-440.
- [2] P. Gütllich, *European Journal of Inorganic Chemistry* **2013**, 581-591.
- [3] a) K. Senthil Kumar and M. Ruben, *Coordination Chemistry Reviews* **2017**, *346*, 176-205; b) A. B. Gaspar, V. Ksenofontov, M. Seredyuk and P. Gütllich, *Coordination Chemistry Reviews* **2005**, *249*, 2661-2676; c) Z.-H. Li, Y.-X. Wang, W.-K. Han, W. Zhu, T. Li, Z. Li, X. Ren and Z.-G. Gu, *New J. Chem.* **2017**, *41*, 10062-10068.
- [4] J.-Y. Zhang, L.-J. Su, Q.-J. Guo and J. Tao, *Inorganic Chemistry Communications* **2017**, *82*, 39-43.
- [5] a) M. Matsuda, H. Isozaki and H. Tajima, *Chemistry Letters* **2008**, *37*, 374-375; b) I. Suleimanov, O. Kraieva, J. S. Costa, I. O. Fritsky, G. Molnar, L. Salmon and A. Bousseksou, *Journal of Materials Chemistry C* **2015**, *3*, 5026-5032; c) I. Suleimanov, O. Kraieva, G. Molnar, L. Salmon and A. Bousseksou, *Chemical Communications* **2015**, *51*, 15098-15101; d) Y. Jiao, J. Zhu, Y. Guo, W. He and Z. Guo, *J. Mater. Chem. C* **2017**, *5*, 5214-5222; e) I. Suleimanov, G. Molnár, L. Salmon and A. Bousseksou, *European Journal of Inorganic Chemistry* **2017**, *2017*, 3446-3451.
- [6] A. Diaconu, S.-L. Lupu, I. Rusu, I.-M. Risca, L. Salmon, G. Molnár, A. Bousseksou, P. Demont and A. Rotaru, *The Journal of Physical Chemistry Letters* **2017**, *8*, 3147-3151.
- [7] J.-X. Hu, Y.-S. Meng, L. Zhao, H.-L. Zhu, L. Liu, Q. Liu, C.-Q. Jiao and T. Liu, *Chemistry - A European Journal* **2017**.
- [8] a) L. a. Piñeiro-López, F. J. Valverde-Muñoz, M. Seredyuk, M. C. Muñoz, M. Haukka and J. A. Real, *Inorganic Chemistry* **2017**, *56*, 7038-7047; b) X. Bao, H. J. Shepherd, L. Salmon, G. Molnar, M. L. Tong and A. Bousseksou, *Angewandte Chemie-International Edition* **2013**, *52*, 1198-1202; c) E. Coronado, M. Gimenez-Marques, G. M. Espallargas, F. Rey and I. J. Vitorica-Yrezabal, *Journal of the American Chemical Society* **2013**, *135*, 15986-15989; d) M. Ohba, K. Yoneda, G. Agusti, M. C. Munoz, A. B. Gaspar, J. A. Real, M. Yamasaki, H. Ando, Y. Nakao, S. Sakaki and S. Kitagawa, *Angewandte Chemie-International Edition* **2009**, *48*, 4767-4771; e) J. A. Real, E. Andres, M. C. Munoz, M. Julve, T. Granier, A. Bousseksou and F. Varret, *Science* **1995**, *268*, 265-267; f) H. T. Xu, Z. L. Xu and O. Sato, *Microporous and Mesoporous Materials* **2014**, *197*, 72-76; g) C. D. Polyzou, N. Lalioti, V. Psycharis and V. Tangoulis, *New J. Chem.* **2017**.
- [9] P. Gütllich and H. A. Goodwin in *Spin Crossover in Transition Metal Compounds I-III*, Vol. Springer Berlin Heidelberg, Berlin, Heidelberg, **2004**.
- [10] P. Gütllich, *European Journal of Inorganic Chemistry* **2013**, 574-1067.
- [11] a) M. M. Dîrtu, A. Rotaru, D. Gillard, J. Linares, E. Codjovi, B. Tinant and Y. Garcia, *Inorganic Chemistry* **2009**, *48*, 7838-7852; b) C. J. Johnson, G. G. Morgan and M. Albrecht, *J. Mater. Chem. C* **2015**, *3*, 7883-7889.
- [12] a) M. Steinert, B. Schneider, S. Dechert, S. Demeshko and F. Meyer, *Inorganic Chemistry* **2016**, *55*, 2363-2373; b) X.-R. Wu, H.-Y. Shi, R.-J. Wei, J. Li, L.-S. Zheng and J. Tao, *Inorganic Chemistry* **2015**, *54*, 3773-3780.
- [13] a) Y.-H. Luo, G.-J. Wen, L.-S. Gu, M.-N. Wang and B.-W. Sun, *Polyhedron* **2017**, *121*, 101-106; b) S. Wang, W.-T. Xu, W.-R. He, S. Takaishi, Y.-H. Li, M. Yamashita and W. Huang, *Dalton Trans.* **2016**, *45*, 5676-5688.
- [14] M. Nihei, Y. Yanai, I. J. Hsu, Y. Sekine and H. Oshio, *Angewandte Chemie International Edition* **2017**, *56*, 591-594.
- [15] a) H. Hagihara, O. Sakaguchi, K. Nishi, S. Hashimoto and N. Matsumoto, *Bulletin of the Chemical Society of Japan* **2011**, *84*, 936-942; b) V. V. Novikov, I. V. Ananyev, A. A. Pavlov, M. V. Fedin, K. A. Lyssenko and Y. Z. Voloshin, *The Journal of Physical Chemistry Letters* **2014**, *5*, 496-500; c) S. Schlamp, K. Dankhoff and B. Weber, *New J. Chem.* **2014**, *38*, 1965-1972; d) S. Vela, J. J. Novoa and J. Ribas-Arino, *Phys. Chem. Chem. Phys.* **2014**, *16*, 27012-27024.
- [16] a) P. L. Franke and W. L. Groeneveld, *Transition Metal Chemistry* **1981**, *6*, 54-56; b) P. L. Franke, J. G. Haasnoot and A. P. Zuur, *Inorganica Chimica Acta-Articles* **1982**, *59*, 5-9.
- [17] a) D. Müller, C. Knoll, B. Stöger, W. Artnner, M. Reissner and P. Weinberger, *European Journal of Inorganic Chemistry* **2013**, 984-991; b) D. Müller, C. Knoll and P. Weinberger, *Monatshefte für Chemie - Chemical Monthly* **2016**, *148*, 131-137.
- [18] a) N. Hassan, P. Weinberger, K. Mereiter, F. Werner, G. Molnar, A. Bousseksou, M. Valtiner and W. Linert, *Inorganica Chimica Acta* **2008**, *361*, 1291-1297; b) M. Valtiner, H. Paulsen, P. Weinberger and W. Linert, *Match-Communications in Mathematical and in Computer Chemistry* **2007**, *57*, 749-761; c) P. J. van Koningsbruggen, M. Grunert and P. Weinberger, *Monatshefte Fur Chemie* **2003**, *134*, 183-198; d) C. M. Grunert, J. Schweifer, P. Weinberger, W. Linert, K. Mereiter, G. Hilscher, M. Müller, G. Wiesinger and P. J. van Koningsbruggen, *Inorganic Chemistry* **2004**, *43*, 155-165.
- [19] P. Weinberger and M. Grunert, *Vibrational Spectroscopy* **2004**, *34*, 175-186.
- [20] E. W. Mueller, J. Ensling, H. Spiering and P. Gütllich, *Inorganic Chemistry* **1983**, *22*, 2074-2078.
- [21] a) A. F. Stassen, E. Dova, J. Ensling, H. Schenk, P. Gütllich, J. G. Haasnoot and J. Reedijk, *Inorganica Chimica Acta* **2002**, *335*, 61-68; b) A. F. Stassen, M. Grunert, E. Dova, M. Müller, P. Weinberger, G. Wiesinger, H. Schenk, W. Linert, J. G. Haasnoot and J. Reedijk, *European Journal of Inorganic Chemistry* **2003**, 2273-2282.
- [22] M. Seifried, C. Knoll, G. Giester, J. M. Welch, D. Müller and P. Weinberger, *European Journal of Organic Chemistry* **2017**, *2017*, 2416-2424.
- [23] P. Gütllich, A. Hauser and H. Spiering, *Angewandte Chemie International Edition in English* **1994**, *33*, 2024-2054.
- [24] D. D. Perrin, W. L. F. Armarego, *Butterworth-Heinemann, Oxford* **1997**.
- [25] D. Müller, C. Knoll, M. Seifried and P. Weinberger, *Vibrational Spectroscopy* **2016**, *86*, 198-205.
- [26] I. Bruker Analytical X-ray Instruments, **2012**.
- [27] M. J. Frisch, G. W. Trucks, H. B. Schlegel, G. E. Scuseria, M. A. Robb, J. R. Cheeseman, G. Scalmani, V. Barone, B. Mennucci, G. A. Petersson, H. Nakatsuji, M. Caricato, X. Li, H. P. Hratchian, A. F. Izmaylov, J. Bloino, G. Zheng, J. L. Sonnenberg, M. Hada, M. Ehara, K. Toyota, R. Fukuda, J. Hasegawa, M. Ishida, T. Nakajima, Y. Honda, O. Kitao, H. Nakai, T. Vreven, J. A. Montgomery Jr., J. E. Peralta, F. Ogliaro, M. J. Bearpark, J. Heyd, E. N. Brothers, K. N. Kudin, V. N. Staroverov, R. Kobayashi, J. Normand, K. Raghavachari, A. P. Rendell, J. C. Burant, S. S. Iyengar, J. Tomasi, M. Cossi, N. Rega, N. J. Millam, M. Klene, J. E. Knox, J. B. Cross, V. Bakken, C. Adamo, J. Jaramillo, R. Gomperts, R. E. Stratmann, O. Yazyev, A. J. Austin, R. Cammi, C. Pomelli, J. W. Ochterski, R. L. Martin, K. Morokuma, V. G. Zakrzewski, G. A. Voth, P. Salvador, J. J. Dannenberg, S. Dapprich, A. D. Daniels, Ö. Farkas, J. B. Foresman, J. V. Ortiz, J. Cioslowski and D. J. Fox in *Gaussian 09*, Vol. Gaussian, Inc., Wallingford, CT, USA, **2009**.
- [28] a) C. T. Lee, W. T. Yang and R. G. Parr, *Physical Review B* **1988**, *37*, 785-789; b) A. D. Becke, *Journal of Chemical Physics* **1993**, *98*, 5648-5652; c) P. J. Stephens, F. J. Devlin, C. F. Chabalowski and M. J. Frisch, *Journal of Physical Chemistry* **1994**, *98*, 11623-11627.
- [29] Ditchfie.R, D. P. Miller and J. A. Pople, *Journal of Chemical Physics* **1971**, *54*, 4186-8.
- [30] a) T. Dunning Jr in *PJ Hay in Modern Theoretical Chemistry*, Vol. 3, *HF Schaefer III*, Ed. Vol. Plenum, New York, **1977**; b) P. J. Hay and W. R. Wadt, *Journal of Chemical Physics* **1985**, *82*, 299-310; c) W. R. Wadt and P. J. Hay, *Journal of Chemical Physics* **1985**, *82*, 284-298.
- [31] W. J. Stevens, H. Basch and M. Krauss, *Journal of Chemical Physics* **1984**, *81*, 6026-6033.

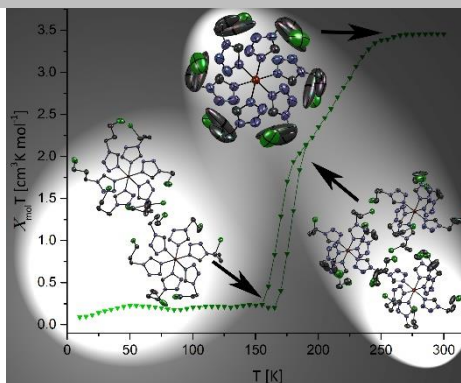
FULL PAPER

Entry for the Table of Contents

Layout 1:

FULL PAPER

A halogen substitution of 1-(propyl)-1*H*-tetrazole was found to shift the spin transition temperature about 70 K towards room-temperature. The reason for this impact was found in the steric fine-tuning of the ligands backbone.



Danny Müller,* Christian Knoll,
Marco Seifried Jan M. Welch, Gerald
Giester, Michael Reissner, Peter
Weinberger

Page No. – Page No.

Halogenated Alkyltetrazoles for
Rational Design of Fe(II)-Spin
Crossover Materials – Fine-tuning
of the Ligands Size